Non-isothermal Crystallization Kinetics of Linear Metallocene Polyethylenes

Ibnelwaleed A. Hussein

Department of Chemical Engineering, King Fahd University of Petroleum & Minerals, Dhahran 31261, Saudi Arabia

ABSTRACT

The effect of Mw on the non-isothermal crystallization kinetics of metallocene linear polyethylene (m-PE) was studied using modulated differential scanning calorimetry. Six linear m-PEs of molecular weights in the range 122-934 kg/mol were prepared by gas phase polymerization. The cooling rate was varied in the range 2^{o}–20^{o}C/min and it has significantly affected the crystallization behavior. The Mw had a weak influence on both the peak crystallization temperature, and the crystallization onset temperature. All m-PEs showed primary and secondary crystallizations. Both at low and high cooling rates, crystallinity showed significant drop (~30%) when Mw was increased from 122 to 934 kg/mol. At low cooling rates (<10^{o}C/min), rate parameters in modified Avrami (k_R) and Mo [F(T)] methods of analyses agree in suggesting that increased Mw slows the rate of crystallization. The Mw dependency of the primary rate constant, k_R, followed Arrhenius type ($k_R = k_{Ro}\, e^{\,281/Mw}$, where k_{Ro} is rate dependent). However, at higher cooling rates k_R approached a constant value. The order parameters obtained by the different methods of analyses (n and α) were independent of Mw suggesting that the crystal type remains the same. Hoffman-Lauritzen theory was used for data analysis and U* showed a significant decrease from 225.0 to 11.8 kJ/mol when the Mw was increased from 152 to 934 kg/mol. Finally, all methods of analysis suggest the significant effect of Mw on slowing the overall crystallization process.

*Key words***:** molecular weight, crystallization kinetics, metallocene polyethylene, non-isothermal crystallization, modulated DSC

Email: ihussein@kfupm.edu.sa; Tel: +966 3 860 2235; Fax: 860 4234

INTRODUCTION:

The investigation of melting and crystallization behaviors of polymers is influenced by the molecular structure. The study of polymer crystallization kinetics is important from theoretical and practical points of view [1-5] and many researchers have studied the crystallization behavior of different polyethylenes [6-11]. The influence of molecular structure and crystallization conditions on the crystallization behavior of ethylene/α-olefin copolymers were studied [12-25]. Most of these studies used Ziegler-Natta polyethylenes (ZN-PE), which are known for their heterogeneity in size and composition [12, 14, 17, 21, 26]. Also, the previous studies used primarily fractions of conventional heterogeneous ZN-PEs. Hence, the effect of the individual structural parameters on the crystallization phenomenon is difficult to separate. Metallocene PEs (m-PEs) have narrow MWD in the range 2-3 and for linear ZN-PE, MWD is the only interfering parameter.

Several studies on the thermal properties and molecular structure of PEs were reported by different authors [22, 25, 27-37]. Most of these studies used linear low density polyethylene (LLDPE) with focus on the influence of short chain branch distribution on melting and crystallization kinetics [22, 27-29, 33, 36, 37], particularly of a single polymer and its fractions using different fractionation techniques [31, 32, 34-36]. Modulated differential scanning calorimetry (MDSC) was the main technique used to study the melting and crystallization kinetics. However, the influence of Mw on the non-isothermal crystallization kinetics of linear m-PEs is yet to be studied. The author feels that the main reason behind that is the difficulty of finding commercial linear m-PE with different Mw. So, in this study experimental resins were prepared to investigate the influence of Mw on the non-isothermal crystallization kinetics of linear m-PE using MDSC.

EXPERIMENTAL

Materials and Sample Preparation

Six linear PE samples were prepared by gas-phase polymerization. Laboratory prepared catalysts were used for all the PE synthesis. For samples M122 to M172, (n-

$BuCp)_2$ $ZrCl_2$ on polymeric support treated with MAO were used. A proprietary non metallocene catalyst was used for the synthesis of samples # M934. The number associated with each sample is the Mw of that sample (see Table 1). The GPC results for sample M934 are not reliable because it was difficult to dissolve the sample and heating to 170°C was required; this resulted in sample deterioration. The columns used are also not well suited for analyzing samples with Mw of as high as those of sample M934. The true Mw of this sample is very likely over one million and the polydispersity is probably close to 2.5 as suggested by Professor S.E. Wanke of the University of Alberta. The molar mass measurements were done with an Alliance GPCV 2000 from Waters, equipped with 3 HT6E columns. Trichlorobenzene was used as the solvent and Millennium software from Waters was used to process the data. The standard has a Mw of 53 kg/mol and PD of 2.9. The synthesis and molar mass characterization of the samples were done in Professor Wanke's laboratory. Prior DSC testing, all powder samples were melt-blended at our laboratory in a Haake melt blender at 190°C and 50 rpm for 10 minutes in the presence of 3000 ppm of extra antioxidant. The main reason for the addition of the antioxidant is to save the polymer from degradation during testing [38].

Modulated Differential Scanning Calorimetry (MDSC)

MDSC measurements were performed using a TA Q1000 instrument equipped with a liquid nitrogen cooling system and auto sampler. Nitrogen at a flow rate of 50 ml/min was used to purge the instrument. Polymer samples (7.5-9.8 mg) were sliced and compressed into non-hermetic aluminum pans. To minimize the thermal lag between the sample and the pan, samples with flat surface were used. An empty aluminum pan was used as reference. The previous thermal effects were removed by heating the samples to 140°C and holding at this temperature for 5 min. All the samples were cooled to subambient temperatures for complete evaluation of crystallization [21]. The samples were cooled from 140°C to 5°C at a rate of 2°C/min (with ± 0.2°C modulation), 4°C/min (with ± 0.4°C modulation) and 6°C/min (with ± 0.6°C modulation) at every 40 s. First, the baseline was calibrated using empty crimped aluminum pans. The melting temperature and heat of fusion were calibrated using a high purity Indium standard (156.6°C and 28.45 J/g). A sapphire disc was used to measure heat capacity. The

absolute crystallinity was calculated using the heat of fusion of a perfect polyethylene crystal, 290 J/g [Ref. 39, pp. 347]. Here, the reversing and non-reversing heat capacity approach [40] was used for data analysis. Data of the non-reversing curve was processed using Universal analysis software (provided by TA Instruments, Inc) to obtain the crystallization parameters.

Non-isothermal crystallization kinetics

Several analytical methods have been developed to describe the non-isothermal crystallization kinetics of polymers: (1) the modified Avrami analysis [1, 41-43]; (2) the Ozawa analysis [1]; (3) Ziabicki analysis [44,45]; and others [46-47]. In this study, the modified Avrami analysis proposed by Jeziorny [2] and the Mo method suggested by Liu et al. [48] were used to describe the non-isothermal crystallization kinetics of m-LLDPEs. Due to the variation in the range of crystallization temperature, Ozawa model [1] was not suitable for this study. The Avrami equation is defined as follows [41-43]:

$$1 - X_t = \exp(-k_t t^n) \tag{1}$$

where n is the Avrami crystallization exponent dependent on the nucleation mechanism and growth dimension, t is the time taken during the crystallization process, k_t is the growth rate constant, which depends on nucleation and crystal growth, and X_t is the relative crystallinity [43]. The relative crystallinity, X_t is defined as follows:

$$X_t = \frac{\int_{t_o}^{t} (dH_c / dt)dt}{\int_{t_o}^{t_\infty} (dH_c / dt)dt} \tag{2}$$

where dH_c/dt is the rate of heat evolution, and t_o and t_∞ are the onset and completion times of the crystallization process, respectively. Avrami equation was developed based on the assumption that the crystallization temperature is constant. Jeziorny [2] modified the equation to describe non-isothermal crystallization. At a chosen cooling rate, relative crystallinity is a function of the crystallization temperature (T). That is, equation 2 can be formulated as:

$$X_T = \frac{\int_{T_o}^{T_c} (dH_c / dT)dT}{\int_{T_o}^{T_\infty} (dH_c / dT)dT} \tag{3}$$

where T_o denotes the onset crystallization temperature, and T_c and T_∞ represent the crystallization temperature at time t and after the completion of the crystallization process, respectively. Crystallization time, t, can be converted from crystallization temperature, T_c, using the following equation [1, 45] (that is strictly valid when the sample experiences the same thermal history).

$$t = \frac{T_o - T}{R} \tag{4}$$

where R is the cooling rate (^oC/min). The double-logarithmic form of equation 1 yields

$$\ln[-\ln[1 - X_t]] = \ln k_t + n \ln t \tag{5}$$

Thus, the Avrami exponent n and the crystallization rate constant k_t can be obtained from the slope and the intercept of the plot of ln[-ln(1-X_c)] vs ln t, respectively, for each cooling rate. The physical meaning of k_t and n cannot be related to the non-isothermal case in a simple way; they provide further insight into the kinetics of non-isothermal crystallization. The rate of non-isothermal crystallization depends on the cooling rate. Therefore, k_t can be corrected to obtain the corresponding rate constant at a unit cooling rate, k_R [1]:

$$\ln k_R = \ln k_t \ / R \tag{6}$$

A method modified by Mo was also employed to describe the non-isothermal crystallization, which combines the Avrami equation with the Ozawa equation. Its final form is given below [48]:

$$\ln R = \ln F(T) - \alpha \ln t \tag{7}$$

where $F(T)=[[k(T)/ k_t]^{1/m}$ represents the value of cooling rate; α is the ratio of the Avrami exponent n to the Ozawa exponent m (α = n/m).

Further, the effective activation energy, ΔE_x, was calculated theoretically using the method proposed by Vyazovkin and Sbirrazzuoli [49]. In this method, the coefficient of the growth rate, G, and the overall crystallization rate, dX/dt, are related by:

$$-E / R = \frac{d \ln G}{dT^{-1}} = \frac{d \ln(dX / dt)}{dT^{-1}} \tag{8}$$

The growth rate G is given as a function of the crystallization temperature, T_c, by Hoffman-Lauritzen equation in the context of the Hoffman-Lauritzen secondary nucleation theory [50]. Vyazovkin and Sbirrazzuoli [49] modified the Hoffman-Lauritzen equation to calculate ΔE_x at a given conversion X from the following relationship:

$$\Delta E_x = U^* \frac{T^2}{(T - T_\infty)^2} + K_g R \frac{(T_m^o)^2 - T^2 - T_m^o T}{(T_m^o - T)^2 T} \quad (9)$$

where U* denotes the activation energy per segment which characterizes molecular diffusion across the interfacial boundary between melt and crystals, T_∞ is usually set equal to (T_g-30) K with T_g being the glass transition temperature of the polymer. K_g is a nucleation constant and T_m^o is the equilibrium melting point for the polymer and R is the gas constant. The Vyazovkin and Sbirrazzuoli method and Hoffman-Lauritzen theory were widely used in the recent literature to calculate U* and K_g [51-54].

RESULTS AND DISCUSSION

Non-isothermal Crystallization

The non-isothermal crystallization MDSC traces (non-reversing curves) of linear m-PE at low and high cooling rates (2 and 20^{o}C/min) are shown in Figures 1 a & b, respectively. The m-PE crystallization exotherms are fairly similar. They show a distinct high temperature peak followed by a minor broad long tail. A primary crystallization was observed at high temperatures and a secondary crystallization at low temperatures. Different parameters obtained from Figure 1 are listed in Table 2. These parameters include: the onset crystallization temperature (T_c^{onset}), which is the temperature at the intersection of the tangents of the baseline and the high temperature side of the exotherm; the peak crystallization temperature (T_c^{peak}); the enthalpy of crystallization (ΔH_c), and absolute crystallinity (X_c). The above parameters were obtained at different cooling rates in the range 2^o-20^{o}C/min.

At low cooling rates (2°C/min), the T_c^{onset} and T_c^{peak} were in the range 124°-125°C and 120° to121°C, respectively. On the other hand, at high cooling rates (20°C/min), the T_c^{onset} and T_c^{peak} were in the range 120°-122°C and 116°-118°C, respectively. So, both T_c^{onset} and T_c^{peak} were shifted to lower values at high cooling rates. However, the cooling rate had a weaker influence on T_c^{onset} in comparison with its influence on T_c^{peak}. Both at low and high cooling rates, X_c showed significant drop (~30%) when Mw was increased from 122 to 934 kg/mol. In addition, the drop in crystallinity as a result of increased cooling rate was < 10%.

The crystallization exotherm data obtained at 2°and 20°C/min are shown in Figure 2 a & b, respectively. The relative crystallinity (X_T) as a function of temperature was calculated using equation 3. Results for all samples and at all rates are given in Table 2. X_T was then converted into X_t by transforming the temperature axis to the time analogue using equation 4. X_t versus crystallization time is plotted in Figure 3 a & b. Initially, an attempt was made to fit the whole data of m-PEs using the Avrami analysis as shown in Figure 4 a &b. Figure 4 a & b represent the Avrami plots of all m-PE at 2, and 20°C/min, respectively. Data at other rates are not shown here; however, the extracted parameters are displayed in Table 3. It is clear that the observed variations in the n values are due to the poor fit of Avrami equation for the whole range as reflected in the regression coefficient. However, this was also observed in all the previous publications that used Avrami equation to fit the whole range of data. Therefore, it is a problem of the used model. On the other hand, the other method of data analysis that uses the activation energy (Hoffman-Lauritzen theory) results in much better fitting since the method assumes activation energy to be temperature dependent.

All m-PEs showed two linear parts. At low cooling rates (at 2° and 5°C/min), the second linear part approaches a plateau, while at high cooling rates (10° and 20°C/min) the linear portion has a more positive slope. It should be noted that all m-PEs are linear molecules with very similar MWD (2-3). Hence, the only explanation for the observation of the second linear part is through primary and secondary crystallization approach suggested by Wunderlich [55]. The mechanism of secondary crystallization is suggested to be either a crystal perfection process or a crystal thickness growth [55]. Similar

deviations in Avrami plots were reported by several authors in similar crystallization studies. For example, see the results of Jiao et al. [Figure 6a of ref. 24]; Janimak and Stevens [Figure 5 of ref. 30] for m-LLDPE and Liu et al. [Figure 7 of ref. 48] for copolyterephthalamide. Janimak and Stevens [30] used a single line to fit the whole set of data applying the least square method.

The values of n, k_t, k_R, and coefficient of determination (r^2) are listed in Table 3. At a cooling rate of 2°C/min, n increased from 2.5 to 3.6 when the Mw was increased from 122 to 934 kg/mol. The average value of n is 3. These values are in agreement with previous literature reports on linear PE that suggest spherulitic growth with the n values in the range of 3 - 4 [56,57]. At high rates (20°C/min), n was in the range 1.6 to 2.6 with an average of 2. The value of n is usually an integer between 1 and 4 for different crystallization mechanisms and a fraction for secondary crystallization [57,58]. Hence, n has a weak cooling rate dependency, which suggests that the type of crystal is likely independent of cooling rate. The fact that our average values of n are either 2 or 3 suggests that we have instantaneous nucleation [59]. The main reason for having fractional n values is the data fitting which is evident in the regression coefficient (see Table 3). For other reasons that can results in fractional n values see the review article by Piorkowska et al. [59]. However, the primary crystallization rate parameters (k_{t1} and k_{R1}), given in Table 3, decreased with increasing Mw at low cooling rates (2° and 5°C/min). The rate constant was sensitive to both Mw and cooling rate. However, at high rates (10° and 20°C/min) k_{R1} is independent of both Mw and cooling rate and approaches a value of 1.1 as shown in Table 3. The Mw dependency of k_{R1} can be fitted by an Arrhenius type relationship ($k_{R1} = k_{Ro}\, e^{281/Mw}$). The values of the constants were found to be rate dependent. At 2°C/min, $k_{R1} = 0.0489\, e^{289/Mw}$ (r^2=0.958), while at 5°C/min, $k_{R1} = 0.1725\, e^{273/Mw}$ (r^2=0.966). The fact that the exponential power is approximately the same, within experimental errors, suggests that the decrease in k_{R1} due to the increase in Mw is an activated state process and the constant (273-289) is related to the activation energy of the primary crystallization. It should be noted that Mw is in kg/mol. In addition, it is noted that the pre-exponential constant is rate dependent, which is the case in Arrhenius type relationships. In general, the Mw dependency of the primary rate constant is similar to the temperature dependency of viscosity.

Further, a kinetic model proposed by Mo [48] was used (see equation 7 above). Plots of ln R vs ln t for all linear m-PE samples are shown in Figure 5 a & b for M122 and M934. Plots for other samples are not shown here; however, the Mo parameters for all samples are given in Table 4. From these plots values of α and F(T) were obtained at different crystallinities in the range 20-80%. All plots were linear as predicted by equation 7. F(T) increased systematically with the increase in percent crystallinity. In general, the higher the Mw the higher is the value of F(T) suggesting the increased difficulty of polymer crystallization. This observation is valid at all levels of crystallization. These results are in agreement with the above observations on k_{R1} obtained through Avrami method. So, both modified Avrami and Mo methods of analysis agree in suggesting increased difficulty of crystallization with increased Mw.

Vyazovkin and Sbirrazzuoli [49] method of analysis (equation 9), which is based on Hoffman-Lauritzen theory for secondary crystallization [50], was used. Samples M155 and M934 were taken as examples of low and high Mw resins. For linear PE, 416.2 K and 153.15 K were used for T_m^o and T_g, respectively [46]. Values of E at different temperatures were obtained by using equation 8. Then, Equation 9 was rewritten in the following format:

$$[E] = U^* [Z] + K_g [Y] \qquad (10)$$

where [E] is the matrix of activation energy data, [Z] and [Y] are the matrices of $[\frac{T^2}{(T-T_\infty)^2}]$ and $[R\frac{(T_m^o)^2 - T^2 - T_m^o T}{(T_m^o - T)^2 T}]$ sets, respectively. MatLab software was used for the solution of the above nonlinear equation. Optimum values of U* and Kg that fit equation 10 were obtained and plotted along with the experimental data in Figure 6. Values of U* were calculated as 11.8 and 240.7 kJ/mol for M934 and M152, respectively. However, K_g was 95.0 and 225.0 for M934 and M152, respectively. The increase in the kinetic parameter Kg due to the increase in Mw may seem to be contradicting the above results from Avrami analysis. However, it should be noted that Hoffman-Lauritzen secondary crystallization theory and Vyazovkin and Sbirrazzuoli [49] method of analysis are different than the Avrami method which is mainly for the primary crystallization part of the data (linear part of the curve). The decrease in the activation energy per segmental jump, U*, from 240.7 to 11.8 kJ/mol with the increase in Mw from

152 to 934 kg/mol suggests that high Mw tends to slow the crystallization process. The decrease in U* is almost 10 times the increase in K_g. Hence, Avrami, Mo and Hoffman-Lauritzen theory methods of analysis agree in suggesting the strong influence of Mw on slowing the overall crystallization process. This decrease is likely due to decreased molecular transport with increased Mw.

CONCLUSIONS

Based on the previous results and discussion, the following can be concluded:

1. The nonisothermal crystallization of linear m-PEs with Mw in the range 122-934 kg/mol occurred through primary and secondary crystallization processes.
2. The Mw had a weak influence on both the peak crystallization temperature, T_c^{peak}, and the crystallization onset temperature, T_c^{onset}. It moved to a lower temperature region as Mw is increased.
3. Both T_c^{onset} and T_c^{peak} shifted to lower values at high cooling rates. However, the cooling rate had a weaker influence on T_c^{onset} in comparison with its influence on T_c^{peak}.
4. Both at low and high cooling rates, crystallinity showed significant drop (~30%) when Mw was increased from 122-934 kg/mol. In addition, the drop in crystallinity as a result of increased cooling rate was < 10%.
5. At low cooling rates (<10^{o}C/min), rate parameters in modified Avrami (k_R) and Mo [F(T)] methods of analyses agree in suggesting that increased Mw slows the rate of crystallization. The Mw dependency of the primary rate constant followed Arrhenius type ($k_R = k_{Ro}\ e^{\ 281/Mw}$, where k_{Ro} is a rate dependent constant). However, at higher cooling rates k_R approaches a constant value.
6. For the primary crystallization, the crystallization constant, n, (calculated using the Avrami analysis modified by Jeziorny) was found to be insensitive to Mw Values of Avrami exponent n depend on cooling rate in agreement with previous literature reports [56-58]. The order parameters obtained by the different methods of analyses (n and α) were independent of Mw suggesting that the crystal type remains the same in the studied range.

7. Vyazovkin and Sbirrazzuoli method of analysis which is based on Hoffman-Lauritzen theory was also used and the activation energy per segmental jump, U*, decreased from 240.7 to 11.8 kJ/mol when the Mw was increased from 152 to 934 kg/mol. The kinetic parameter, K_g, increased from 95.0 to 225.0 when the Mw was increased from 152 to 934 kg/mol. Therefore, the decrease in the segmental activation energy is more significant than the increase in the kinetic parameter K_g. The results of the Hoffman-Lauritzen theory are in agreement with Avrami and Mo methods of analysis. All methods suggest the strong influence of high Mw on slowing the crystallization process.

Acknowledgement

The authors are grateful to King Abdul Aziz City for Science and Technology (KASCT) for providing financial support for this research under research Grant # AT-22-16. The author is thankful to Professor S.E Wanke of the Chemical and Materials Engineering Department at University of Alberta, Canada for providing the samples and the molecular mass data. Further, the support of King Fahd University of Petroleum & Minerals (KFUPM) is also acknowledged. Thanks to Mr. Ashraful Islam for his help.

Reference:

[1] Ozawa, T. Polymer 1971, 12, 150.

[2] Jeziorny A. Polymer 1978, 19, 1142.

[3] Jayakannan M, Ramakrishnan S. J Appl Polym Sci 1999, 74, 59.

[4] Sajkiewicz P, Carpaneto L, Wasiak A. Polymer 2001, 42, 5365.

[5] Qui Z, Ikehara T, Nishi T. Polymer 2003, 44, 5429.

[6] Kao YH, Phillips PJ. Polymer 1986, 27, 1669.

[7] Phillips PJ, Kao YH. Polymer 1986, 27, 1679.

[8] Nordmeier E, Lanver U, Lechner MD. Macromolecules 1990, 23, 1072.

[9] Sutton SJ, Vaughan AS, Bassett DC. Polymer 1996, 37, 5735.

[10] Wagner J, Abu-Iqyas S, Monar K, Phillips PJ. Polymer 1999, 40, 4717.

[11] Wagner J, Phillips PJ. Polymer 2001, 42, 8999.

[12] Mandelkern L, Maxfield J. J Polym Sci: Polym Phys Ed 1979, 17, 1913.

[13] Strobl GR, Engelke T, Maderek E, Urban G. Polymer 1983, 24, 1585.
[14] Maderek E, Strobl GR. Colloid Polym Sci 1983, 261, 471.
[15] Alamo R, Domszy R, Mandelkern L. J Phys Chem 1984, 88, 6587.
[16] Mandelkern L. Polym J 1985, 17, 337.
[17] Usami T, Gotoh Y, Takayama S. Macromolecules 1986, 19, 2722.
[18] Alamo RG, Mandelkern L. Macromolecules 1989, 22, 1273.
[19] Fatou JG, Marco C, Mandelkern L. Polymer 1990, 31, 1685.
[20] Alamo RG, Viers BD, Mandelkern L. Macromolecules 1993, 26, 5740.
[21] Shanks RA, Amarasinghe G. J. Therm Anal Calorim 2000, 59, 471.
[22] Zhang M, Lynch DT, Wanke SE. Polymer 2001, 42, 3067.
[23] Rabiej S, Goderis B, Janicki J, Mathot VBF, Koch MHJ, Groeninckx G, Reymaers H, Gelan J, Wlochowicz A. Polymer 2004, 45, 8761.
[24] Jiao C, Wang Z, Liang X, Hu Y. Polym Test 2005, 24, 71.
[25] Bensason S, Minick J, Moet A, Chum S, Hiltner A, Baer E. J Polym Sci: Polym Phys Ed 1996, 34, 1301.
[26] Voigt-Martin IG, Alamo R, Mandelkern L. J Polym Sci: Polym Phys Ed 1986, 24, 1283.
[27] Keating MY, Lee IH. J Macromol Sci Phys 1999, B38, 379.
[28] Starck P, Lehmus P, Seppala V. Polym Engng Sci 1999, 39, 1444.
[29] Xu J, Xu X, Feng L. Eur Polym J 1999, 36, 685.
[30] Janimak JJ, Stevens GC. Termochim Acta 1999, 332, 125.
[31] Razavi-Nouri M, Hay JN. Polymer 2001, 42, 8621.
[32] Fu Q, Chiu F, He T, Liu J, Hsieh ET. Macromol Chem Phys 2001, 202, 927.
[33] Wang C, Chu MC, Lin TL, Lai SM, Shih HH. Polymer 2001, 42, 1733.
[34] Chiu F, Fu Q, Peng Y, Shih H. J Polym Sci, Part B: Polym Phys 2002, 40, 325.
[35] Starck P, Löfgren B. Eur Polym J 2002, 38, 97.
[36] Teng H, Shi Y, Jin X. J Polym Sci, Part B: Polym Phys 2002, 40, 107.
[37] Hussein IA. Polym Int 2004, 53, 1327.
[38] Hameed T, Hussein IA. Polymer 2002, 43, 6911.

[39] Wunderlich B. In: Turi EA, editor. Thermal Characterization of Polymeric Materials, 2nd Edition, vol. 1. New York: Academic Press, 1997.

[40] Schawe JEK. Thermochim Acta 1995, 260, 1.

[41] Avrami M. J Chem Phys 1939;7:1103.

[42] Avrami M. J Chem Phys 1940, 8, 212.

[43] Avrami M. J Chem Phys. 1941, 9, 177.

[44] Ziabbicki A. Colloid Polym Sci 1974, 6, 252.

[45] Ziabbicki A. Appl Polym Symp 1967, 6, 1.

[46] Wunderlich B. Macromolecular Physics, vol. 2. New York: Academic Press, 1976. pp. 147.

[47] Tanem BS, Stori A. Polymer 2001, 42, 5389.

[48] Liu TX, Mo ZS, Wang SE, Zhang HF. Polym Eng Sci 1997, 37, 568.

[49] Vyazovkin S, Sbirrazzuoli N. Macromol Rapid Commun 2004, 25, 733.

[50] Hoffman JD, Davis GT, Lauritzen JI, Jr., in: ‘‘Treatise on Solid State Chemistry’’,Vol. 3, N. B. Hannay, Ed., Plenum Press, New York 1976, chapter 7.

[51] Achilias DS, Papageorgiou GZ, Karayannidis GP. Macromol Chem Phys 2005, 206, 1511.

[52] Cai J, Li T, Han Y, Zhuang Y, ZhANG X. J Appl Polym Sci 2006, 100, 1479.

[53] Vyazovkin S, Dranca I. Macromol Chem Phys 2006, 207, 20.

[54] Botines E, Puiggali J. Euro Polym J 2006, 42, 1595.

[55] Wunderlich B. Macromolecular Physics, vol. 2. New York: Academic Press, 1976. pp. 147.

[56] Buchdahl R, Miller RL, Newman S. J Polym Sci 1959, 36, 215.

[57] Chen K, Tang X, Shen J, Zhou Y, Zhang B. Macromol Mat Engng 2004, 289, 539.

[58] Maderek E, Strobl GR. Colloid Polym Sci 1983, 261, 471.

[59] PiorkowskE, Galeski A, Haudin J-M. Prog Polym Sci 2006, 31, 549.

List of Tables:

Table 1

Resin	Ethylene added, psi	Hydrogen added	Temp., ^{o}C	$M_{w,}$ kg/mol	M_w/M_n
M122	200	Yes	80	121.8	2.34
M155	200	Yes	70	155.1	2.07
M160	200	No	60	160.0	2.35
M169	200	No	60	169.4	2.17
M172	200	No	80	171.6	2.12
M934	100	No	50	934	2.86
Standard				49.6	2.95

Table 2

R (^{o}C/min)	Resin	T_c^{onset} (^{o}C)	T_c^{peak} (^{o}C)	ΔH_c (J/g)	X_c (%)
2	M122	124.2	121.11	184.6	63.64
	M155	124.0	120.93	172.3	59.72
	M160	124.0	120.98	169.6	58.49
	M169	124.0	121.14	170.1	58.65
	M172	124.1	120.15	163.3	56.31
	M934	125.2	122.89	128.9	44.44
5	M122	122.50	120.70	179.9	62.05
	M155	120.8	116.85	168.1	57.97
	M160	123.1	119.29	163.7	56.44
	M169	121.2	116.68	160.76	55.43
	M172	122.6	119.57	162.3	55.95
	M934	124.1	121.46	124.1	42.78
10	M122	121.5	119.31	168.8	58.22
	M155	121.0	118.37	162.3	55.96
	M160	121.5	117.56	154.3	53.22
	M169	121.5	117.91	153.2	52.81
	M172	121.0	118.03	150.6	51.94
	M934	123.1	120.02	116.2	40.08
20	M122	121.0	117.8	172.0	59.31
	M155	120.0	116.95	164.2	56.63
	M160	121.0	115.75	156.2	53.88
	M169	120.5	116.61	158.1	54.51
	M172	120.5	115.76	147.2	50.76
	M934	122.0	118.12	117.9	40.66

Table 3

Cooling Rate (°C/min)	Resin	Primary crystallization			
		n_1	k_{t1}	k_{R1}	r^2
2	M122	2.53	0.172	0.415	0.74
	M155	2.76	0.131	0.362	0.84
	M160	2.76	0.106	0.325	0.89
	M169	2.96	0.094	0.307	0.88
	M172	3.00	0.066	0.257	0.96
	M934	3.61	0.004	0.061	0.93
5	M122	1.64	2.317	1.522	0.77
	M155	2.19	1.022	1.011	0.99
	M160	2.45	1.025	1.012	0.94
	M169	2.45	0.757	0.87	0.97
	M934	3.8	0.051	0.226	0.93
10	M122	1.83	6.945	1.214	0.81
	M155	1.9	6.199	1.2	0.93
	M160	1.99	4.152	1.153	0.97
	M169	1.98	4.848	1.171	0.96
	M172	2.06	4.622	1.165	0.96
	M934	3.78	0.604	0.951	0.94
20	M122	1.55	8.341	1.112	0.79
	M155	1.63	10.35	1.124	0.92
	M160	1.77	8.925	1.116	0.97
	M169	1.81	9.808	1.121	0.94
	M172	2.02	9.734	1.121	0.96
	M934	2.63	5.111	1.085	0.96

Table 4

Resin	Variable	X(t) (%)			
		20	**40**	**60**	**80**
M122	α	0.927	0.961	1.048	1.160
	F(T)	2.276	2.431	2.963	4.907
	r^2	0.937	0.927	0.934	0.957
M155	α	0.856	0.909	0.979	1.078
	F(T)	2.602	3.178	3.96	5.619
	r^2	0.991	0.981	0.980	0.986
M160	α	0.932	1.032	1.112	1.171
	F(T)	2.78	3.381	4.310	6.339
	r^2	0.997	0.998	0.998	0.997
M169	α	0.903	0.964	1.035	1.124
	F(T)	2.915	3.573	4.491	6.453
	r^2	0.988	0.980	0.980	0.989
M172	α	0.976	1.026	1.085	1.166
	F(T)	2.766	3.452	4.376	6.288
	r^2	0.974	0.970	0.971	0.975
M934	α	0.993	1.027	1.060	1.071
	F(T)	7	8.238	10.04	13.3
	r^2	0.987	0.992	0.996	1.00

List of Figures:

Figure # 1

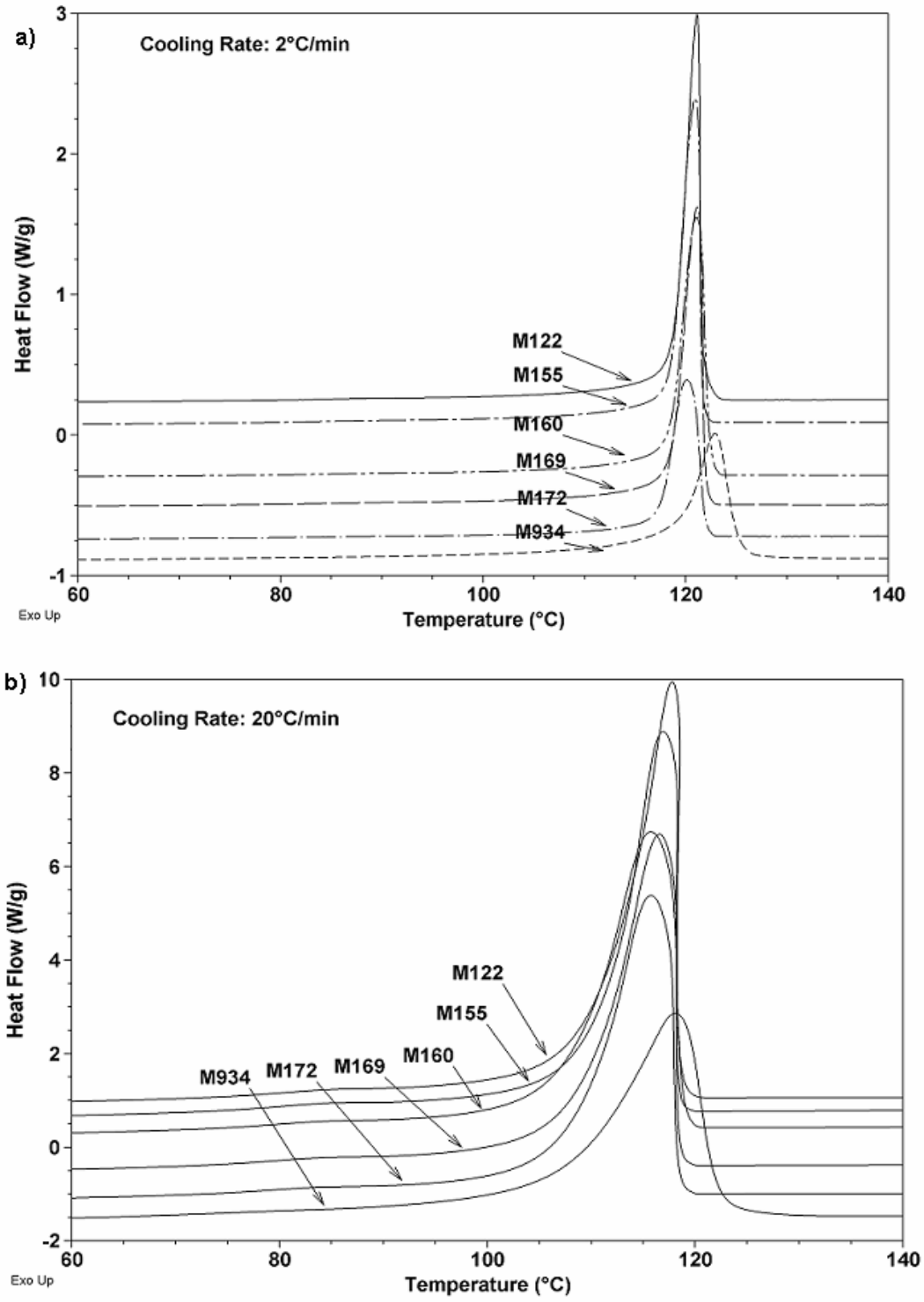
a)
Cooling Rate: 2°C/min
Heat Flow (W/g)
Exo Up
Temperature (°C)
M122
M155
M160
M169
M172
M934
b)
Cooling Rate: 20°C/min
Heat Flow (W/g)
Exo Up
Temperature (°C)
M122
M155
M160
M169
M172
M934

Figure # 2:

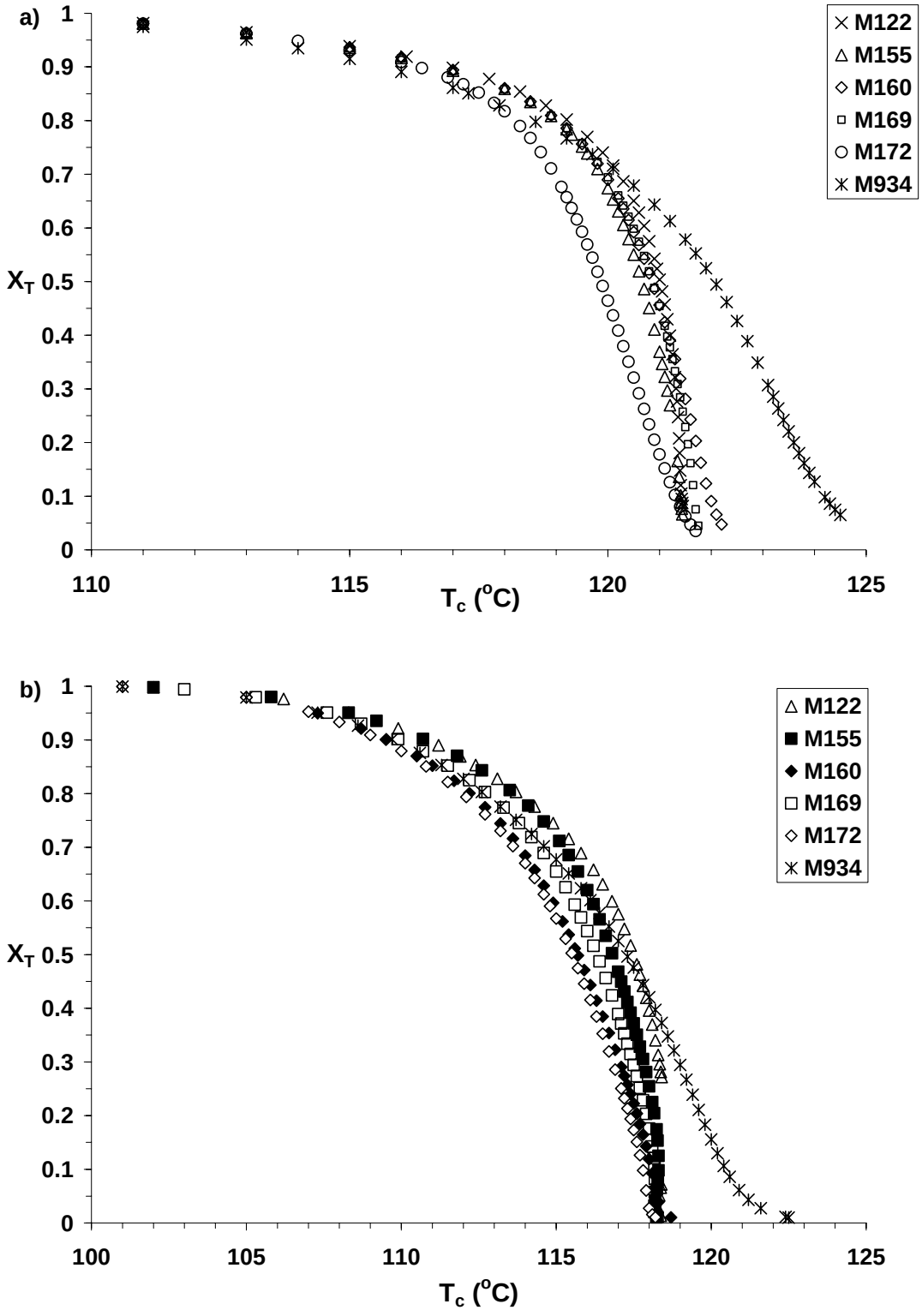
a)
b)
M122
M155
M160
M169
M172
M934
X_T
T_c (^{o}C)
0
0.1
0.2
0.3
0.4
0.5
0.6
0.7
0.8
0.9
1
100
105
110
115
120
125

Figure # 3:

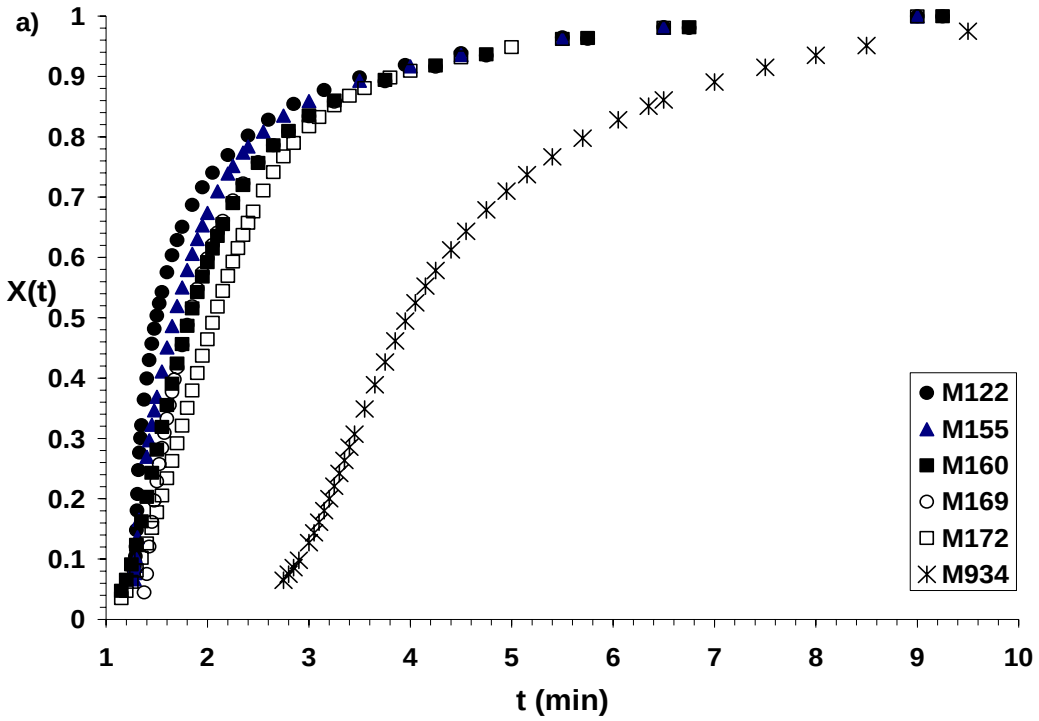
a)
X(t)
t (min)
M122
M155
M160
M169
M172
M934

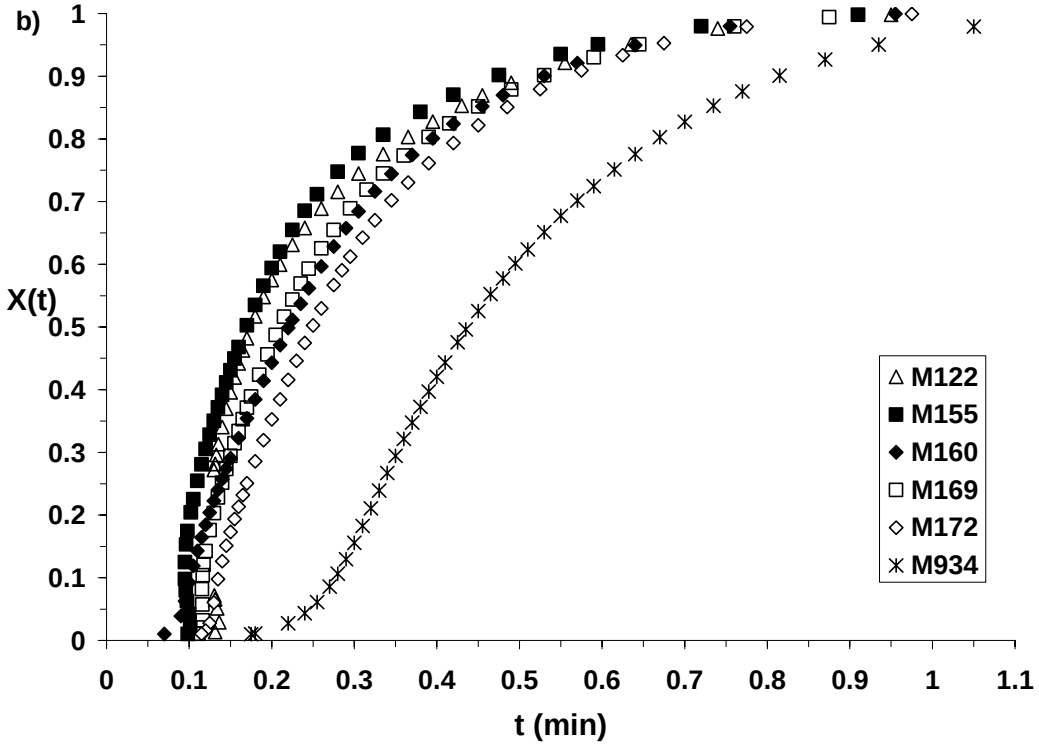
b)
X(t)
t (min)
M122
M155
M160
M169
M172
M934

Figure # 4:

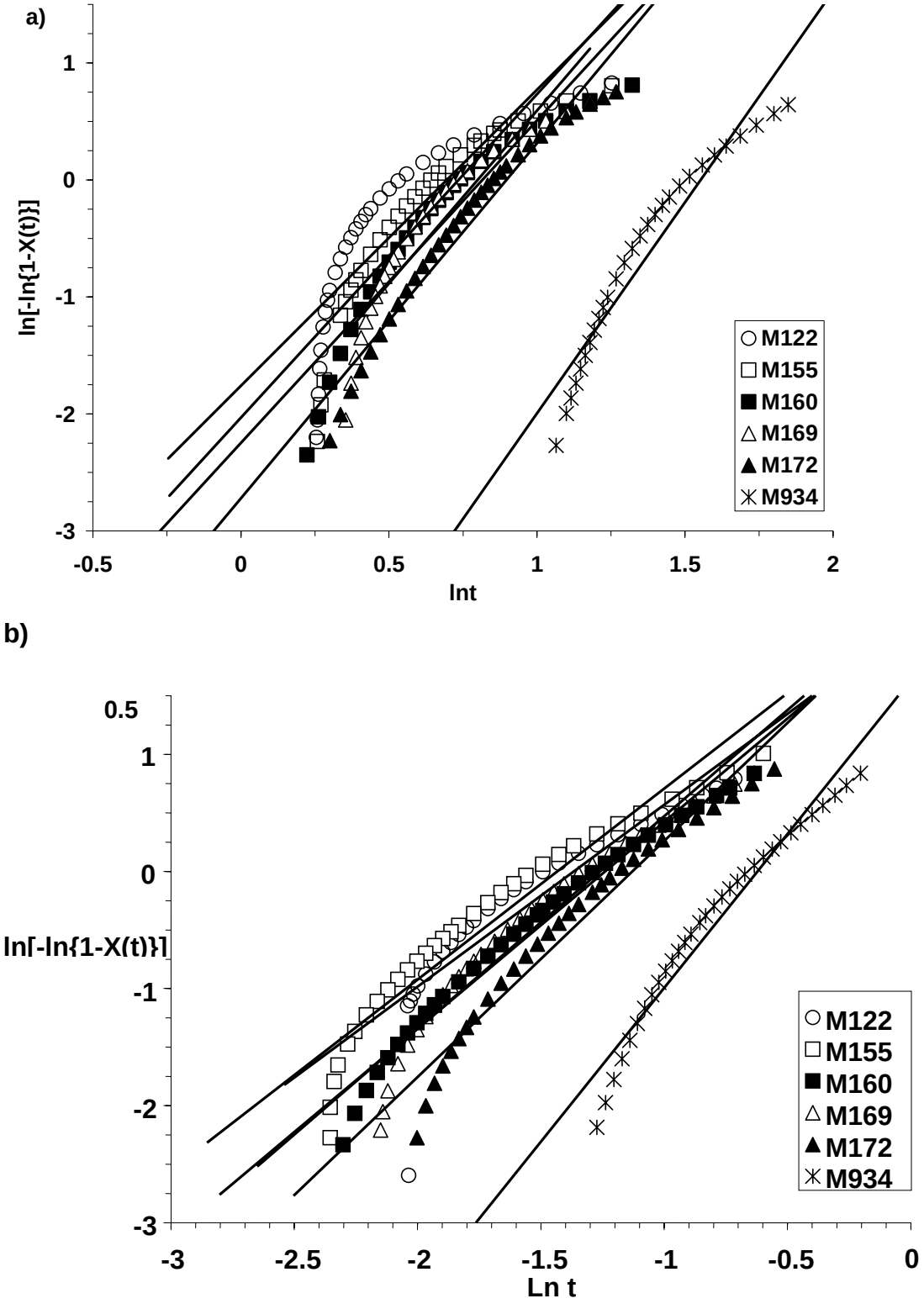
a)
ln[-ln{1-X(t)}]
lnt
M122
M155
M160
M169
M172
M934
b)
ln[-ln{1-X(t)}]
Ln t
M122
M155
M160
M169
M172
M934

Figure # 5:

a)

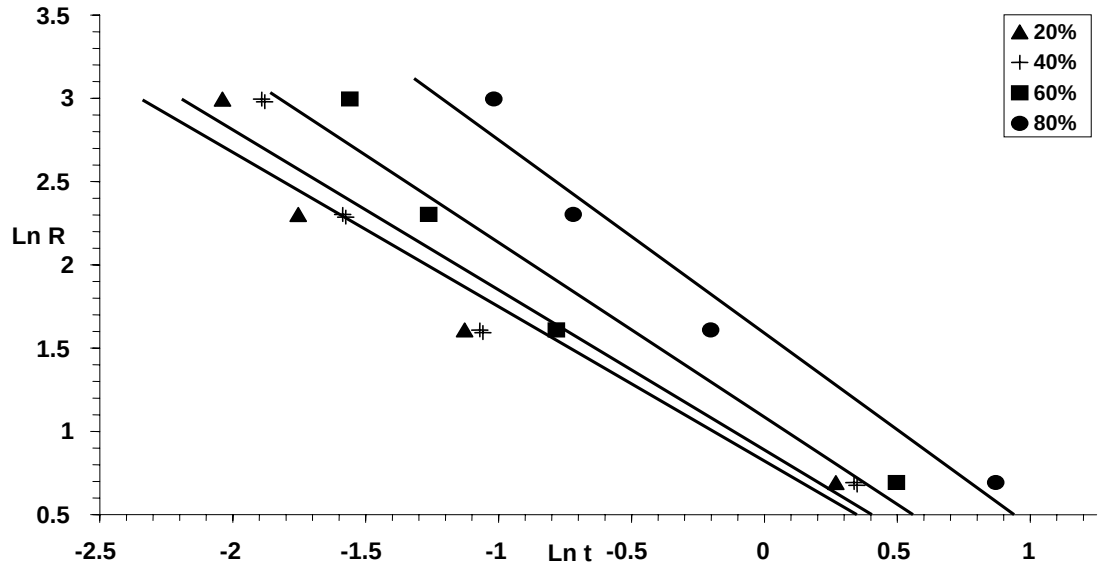
3.5
3
2.5
Ln R
2
1.5
1
0.5
-2.5
-2
-1.5
-1
Ln t
-0.5
0
0.5
1
20%
40%
60%
80%

b)

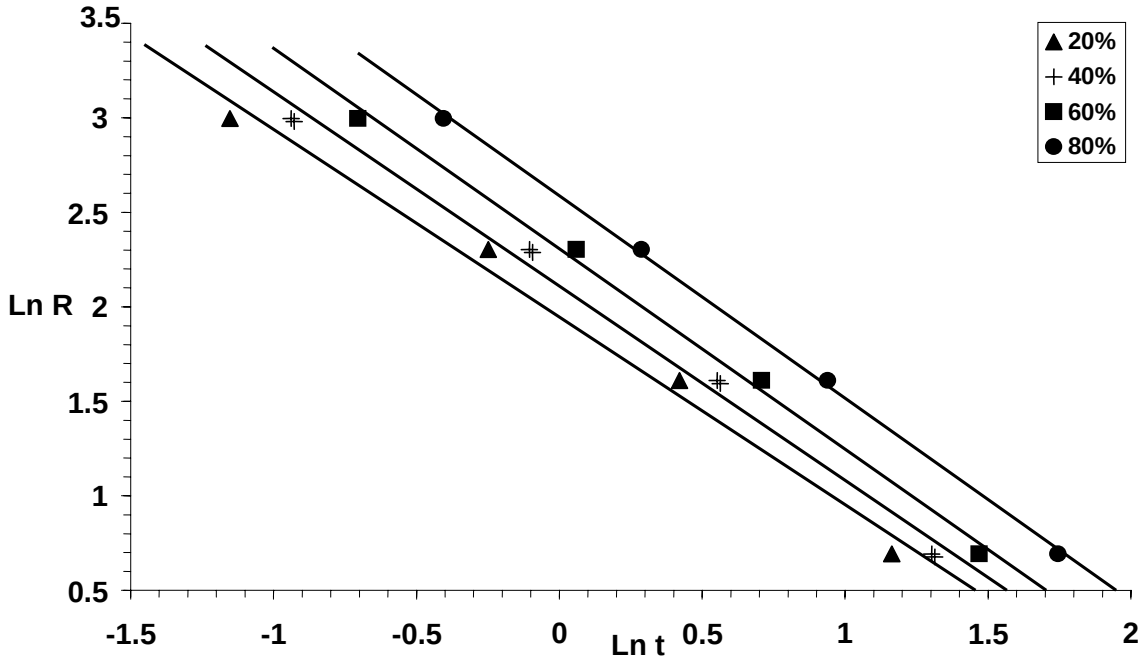
3.5
3
2.5
Ln R
2
1.5
1
0.5
-1.5
-1
-0.5
0
Ln t
0.5
1
1.5
2
20%
40%
60%
80%

Figure 6

a)

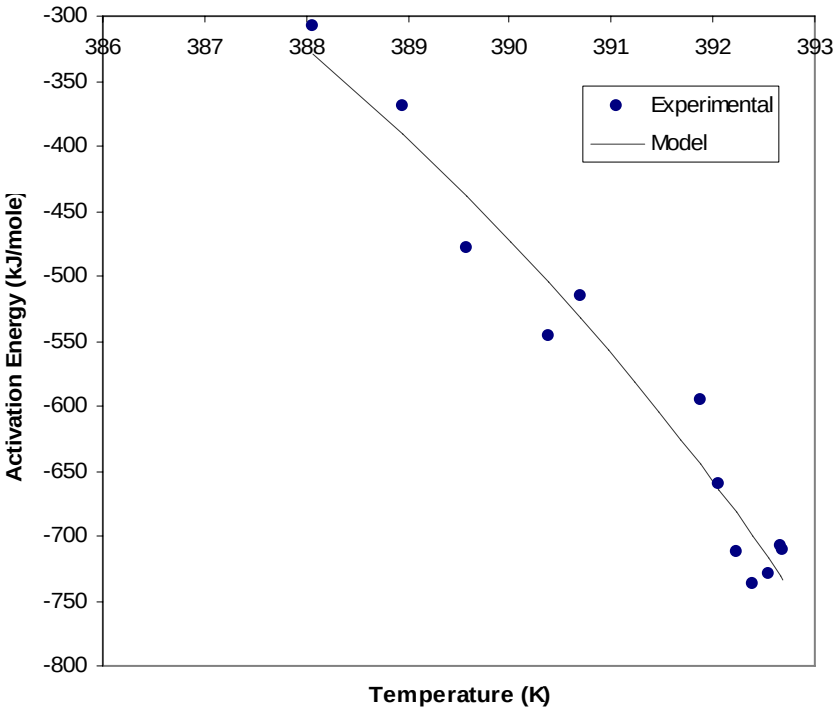
-300
-350
-400
-450
-500
-550
-600
-650
-700
-750
-800
386
387
388
389
390
391
392
393
Experimental
Model
Activation Energy (kJ/mole)
Temperature (K)

b)

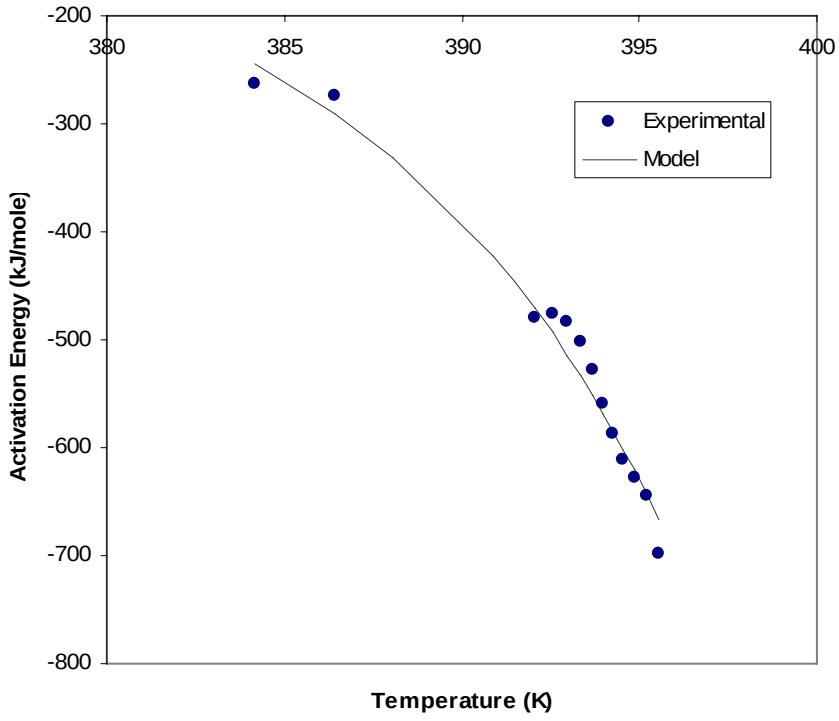
-200
-300
-400
-500
-600
-700
-800
380
385
390
395
400
Experimental
Model
Activation Energy (kJ/mole)
Temperature (K)